Dislocation motion in the presence of diffusing solutes: A computer simulation study

Article *in* Acta Materialia · May 2000

DOI: 10.1016/S1359-6454(00)00035-5

4 authors, including:

D.J. Srolovitz
University of Pennsylvania
593 PUBLICATIONS **25,524** CITATIONS

SEE PROFILE

J. M. Rickman
Lehigh University
151 PUBLICATIONS **2,332** CITATIONS

SEE PROFILE

PERGAMON

Acta mater. 48 (2000) 2163–2175

Acta MATERIALIA

www.elsevier.com/locate/actamat

DISLOCATION MOTION IN THE PRESENCE OF DIFFUSING SOLUTES: A COMPUTER SIMULATION STUDY

Y. WANG[1], D. J. SROLOVITZ[2]†, J. M. RICKMAN[3] and R. LESAR[4]

[1]Department of Materials Science and Engineering, The University of Michigan, Ann Arbor, MI 48109, USA, [2]Princeton Materials Institute and Department of Mechanical and Aerospace Engineering, Princeton University, Princeton, NJ 08544, USA, [3]Department of Materials Science and Engineering, Lehigh University, Bethlehem, PA 18015, USA and [4]MST-8, Los Alamos National Laboratory, Los Alamos, NM 87545, USA

(Received 26 October 1999; accepted 22 January 2000)

Abstract—A discrete lattice, kinetic Monte Carlo model is developed to simulate the motion of an edge dislocation in the presence of interacting, diffusing solute atoms that have a misfit with respect to the matrix. The simulation self-consistently determines the solute concentration profile (in two spatial dimensions), as well as the associated dislocation velocity. The solute segregation profile around the moving dislocation is characterized at low velocity by a condensed solute cloud near and on one side of the dislocation core, a region depleted of solute on the opposite side and a diffuse solute (Cottrell) atmosphere further from the core. At high velocity, no condensed solute cloud forms. The relation between the dislocation velocity and the applied stress shows a low-velocity, solute drag branch and a high-velocity branch, typified by no solute cloud but with occasional solute trapping. At intermediate velocities, the dislocation stochastically jumps between these two branches.

Keywords: Dislocation mobility; Diffusion; Defects; Portevin–LeChatelier effects

1. INTRODUCTION

The interactions of solute atoms with dislocations play a key role in determining how metals will deform. For example, the addition of solutes to an otherwise pure metal invariably produces an alloy that is stronger than the pure metal [1–3]. Analyses of related phenomenon [4–9] suggest that at low driving forces dislocations are effectively pinned by solutes, while at high driving forces the dislocation motion is unimpeded by the solute. The interaction of dislocations with solutes is also responsible for strain-aging phenomena [10] and its dynamic counterpart at elevated temperature, the Portevin–LeChatelier effect [11,12]. Both of these phenomena depend on the tendency of solute atoms to segregate to or be repelled from a dislocation and to diffuse in response to the resultant forces. The more time the solute has to diffuse in response to the solute–dislocation interaction, the stronger will be the effect of solute on dislocation motion. The actual distribution of solute around the dislocation depends on the dislocation velocity, which in turn is determined by the solute distribution. Therefore, the dislocation velocity and solute distribution must be calculated self-consistently. In this paper, we describe a new simulation method for self-consistently obtaining the full two-dimensional solute distribution and the dislocation velocity. Our Monte Carlo model allows for stochastic solute diffusion, the formation of a condensed solute cloud near the dislocation core and a diffuse (Cottrell) solute atmosphere around the dislocation.

The determination of the steady-state substitutional solute concentration about a single edge dislocation in uniform glide motion was considered in detail by Cottrell and Jaswon [13], and later by Yoshinage and Morozumi [14], Hirth and Lothe [15], Takeuchi and Argon [16] and Fuentes-Samaniego *et al.* [17]. In those investigations, the solute atoms were modeled as misfitting spheres in an infinite isotropic linear elastic medium. The choice of chemical potential for the solute essentially is an assumption that the site occupancy of solutes is governed by Boltzmann statistics. Hirth and Lothe [15] pointed out that no more than one substitutional

† To whom all correspondence should be addressed.

1359-6454/00/$20.00
PII: S1359-6454(00)00035-5

solute should be allowed to occupy a given atomic site at a time (i.e. a site exclusion principle must be taken into account). Therefore, the statistical mechanics of the solute distribution must be done in the framework of Fermi–Dirac statistics, which ensures that the atomic solute concentration nowhere exceeds unity. James and Barnett [18] considered the equilibrium distribution of solute around an edge dislocation using Fermi–Dirac statistics and found that the degree of solute pinning depends sensitively on the form of the solute–dislocation interaction within the dislocation core.

When solute atoms are free to diffuse, the concept of dislocation pinning by solutes becomes ambiguous. At low applied stress (i.e. low driving forces for dislocation glide), the solute atoms are able to diffuse along with the moving dislocation. This co-diffusion results in a non-random spatial distribution of solutes and a retarding force on the dislocation. At large driving forces, however, the solute cannot diffuse quickly enough to move along with the dislocation, leading to a distribution of solute that is only slightly disturbed by the dislocation and thus results in a negligible retarding force on the dislocation. When the applied stress field changes, the dislocation velocity changes, leading to a modification of the solute distribution and concomitant retarding force. The result is a non-linear dependence of the dislocation velocity on the applied stress. Therefore, the system may exhibit hysteresis, as suggested by earlier work on the motion of defects in the presence of diffusing solutes [5, 8, 9]. All earlier analyses made severe approximations regarding one or more of the following: choice of ensemble, dimensionality, treatment of the dislocation core, etc.

In this paper, dilatational solute interacts with a gliding edge dislocation in two spatial dimensions, while diffusing in accordance with a Monte Carlo algorithm that incorporates the aforementioned site exclusion. A Monte Carlo algorithm is also used to describe the dislocation motion in response to an applied stress and (potentially) retarded by the solute/dislocation interactions. In the discussion below, we first outline the simulation method employed in these calculations. Then, we examine two limiting cases, the situation in which the dislocation is immobile, but solute atoms are free to diffuse, and the case in which the dislocation is driven by the applied stress in the absence of solute. These limiting cases provide a means of validating the simulation methodology. We next consider the case which is the main focus of this paper, the interaction between diffusing solute and a driven dislocation. In particular, we examine the distribution of solutes around the dislocation as a function of applied stress, the relation between the applied stress and the dislocation velocity, and the source of hysteretic dislocation dynamics in a system containing mobile solute atoms.

2. SIMULATION METHOD

In the present simulations, we present results from simulations where we assume that the misfitting (substitutional) solute atoms create a hydrostation dilatation of the lattice of size ΔV. We include a single dislocation in the simulation, which interacts with the strain field of the solute and the solute atoms diffuse in response to the hydrostatic pressure field of the dislocation. In an external stress field that couples to the dislocation, the dislocation moves in response to the force due to both the solutes and the applied stress.

Both the dislocation and solute atoms are constrained to move on the sites of a square lattice. The lattice parameter is equal to the magnitude of the Burgers vector of the dislocation b. Initially, the dislocation is placed in the center of the two-dimensional simulation cell and the solutes are distributed randomly on the lattice, subject to the restriction that no two solute atoms occupy the same site. The number of solute atoms in the system, N_s, and the solute concentration C_0 are related by $C_0 = N_s/WH$, where W and H are the width and height of the simulation cell (in units of Burgers vectors). Figure 1 is a schematic illustration of the simulation cell.

An external stress that couples to the edge dislocation may be applied to the simulation cell. We arbitrarily choose the Burgers vector to lie parallel to the x-axis. Such a dislocation will then glide in response to a shear stress $\sigma_{xy} = \sigma$ (see Fig. 1). The energy (work) associated with the glide of the dislocation in response to the stress by a distance Δx is $E_\sigma = \sigma b \Delta x$.

The energy associated with the interaction between the stress field of the dislocation and a solute atom is given by $E_s(x, y) = P\Delta V = P(V_s - V_a)$, where P is the pressure field associ-

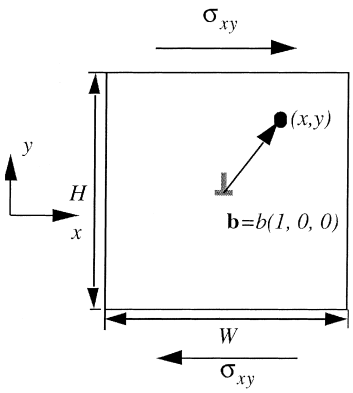

Fig. 1. Schematic illustration of the simulation cell.

ated with the dislocation and V_s and V_a are the volumes of the solute and solvent atoms, respectively. The pressure and energy depend on the position of the solute relative to the dislocation (in the coordinates of Fig. 1)

$$P = \frac{Gb(1+\nu)}{3\pi(1-\nu)} \frac{y}{x^2+y^2}, \tag{1}$$

where G is the isotropic shear modulus and ν is the Poisson's ratio of the material. Since the dislocation stress field decays very slowly with distance and because the present simulations are performed in a simulation cell with periodic boundary conditions in both the x- and y-directions, images of the dislocation must be considered. These images, along with the dislocation itself, form a two-dimensional dislocation array with spacing W and H in the x- and y-directions, respectively.

We can analyze the stresses associated with the dislocation and all of its images using the solution for a linear array of dislocations in Ref. [15]. The total pressure at an arbitrary point in the lattice, associated with a dislocation and all of its images, is then obtained by summing the pressure from a single linear array of dislocations in the y-direction over all dislocation arrays

$$P = \frac{Gb(1+\nu)}{3H(1-\nu)} \sum_{n=-\infty}^{\infty} \frac{\sin 2\pi Y}{\cosh 2\pi\left(X - n\frac{W}{H}\right) - \cos 2\pi Y}, \tag{2}$$

where W is the horizontal spacing between dislocation lines and is also equal to the width of the simulation cell and $X = x/W$ and $Y = y/H$. This expression for the pressure is exact and the summation converges rapidly. Therefore, we truncate this summation by including only the $-4 \le n \le 4$ terms. Increasing this range to ± 5 only changes P by $6 \times 10^{-6}\%$.

Several assumptions are made in the present simulation. First, we explicitly assume that the solutes are pure misfit solutes (i.e. point sources of dilatation). In this case, the solutes do not interact with each other. We further assume that only one solute atom can occupy a lattice site at one time (i.e. Fermi–Dirac statistics are appropriate rather than Boltzmann statistics). Dislocations are assumed to be free to glide in the direction parallel to their Burgers vector (the x-direction in these simulations) and no climb is possible. If the dislocation moves beyond the border of the simulation cell, it reappears at the opposite border of the simulation cell (i.e. periodic boundary conditions). There is no interaction between solute and dislocation when they occupy the same lattice site. This implies a core size of a single interatomic separation. While this is somewhat smaller than most published estimates for metals (see [15]), this does not raise serious problems, as discussed at length below. Modeling the dislocation as a point in two dimensions rather than as a line in three dimensions explicitly excludes the effect of dislocation bow out, which may be important for determining the precise stress at which a dislocation escapes its pinning solute cloud.

It is convenient to work with reduced units for the energy, distance, etc. In the results presented below, we choose to normalize all lengths by the magnitude of the Burgers vector b. Because the simulations are performed in two spatial dimensions, it is convenient to normalize the energy scale by the dislocation quantity Gb^2, which has dimensions of energy per unit length. The external stress is reported directly in units of G. The time will be reported in units of the minimum time required for the dislocation to advance by one Burgers vector, $1/\Gamma$, as discussed below.

In a real material, solute atoms and dislocations can move simultaneously, with distinct mobilities. It is most convenient in the present Monte Carlo simulations to attempt to move only one entity (a single dislocation or solute atom) at a time. The mobilities of solute atoms and dislocations will, in general, be much different. To account for this, we define a mobility ratio as $M_r = M_s/M_d$, where M_d is the dislocation mobility and M_s is the solute atom mobility. This quantity represents the relative frequency with which we try to move a single solute atom relative to that for the movement of the dislocation. We further define the quantity $R = 1 + N_s M_s/M_d$, where N_s is the number of solute atoms in the simulation cell and $1/R$ is the probability of moving the dislocation in a single Monte Carlo step. Since we defined the fundamental time unit as the reciprocal of the dislocation attempt rate, the solute atom attempt rate is M_r times the dislocation attempt rate. There are N_s solute atoms, so that in a single Monte Carlo step the probability of moving any single solute atom is $1\text{-}1/R$. During each Monte Carlo step, we generate a random number in the domain $[0, R)$. If this number is smaller than 1, we attempt to move the dislocation. Otherwise, we randomly choose one of the solute atoms and try to move it. The rationale for this algorithm is that the probability that a random number within $[0, R)$ is smaller than 1 is $1/R$.

Since the edge dislocation is restricted to glide on a single slip plane, we randomly choose whether to let the dislocation attempt to move in the positive or negative direction along the slip plane (i.e. the x-direction—see Fig. 1). The solute atom is free to move in any direction within the two-dimensional square lattice. We calculate the change in energy of the system, ΔE, when a solute atom (or dislocation) moves. If a random number in the range [0, 1) is smaller than the Metropolis function

$$B = \min\left[1, \exp\left(-\frac{\Delta E}{kT}\right)\right], \tag{3}$$

the attempted move is accepted.

Since we are using periodic boundary conditions, an applied stress may force the dislocation to move across the simulation cell and traverse the simulation cell boundary. When the dislocation re-enters the simulation cell on the opposite boundary, it will encounter a distribution of solutes that has already been modified by the dislocation in previous cycles through the simulation cell. This is inappropriate, because in real materials the probability that a single dislocation will traverse exactly the same point in the material traversed by a periodic train of previous dislocations is extremely small. We address this problem by randomizing the spatial distribution of solutes away from the moving dislocation. To minimize any errors associated with this randomization, we choose to randomize the solute positions at a distance as large as possible from the moving dislocation, given the constraints of our simulation cell. This randomization takes place following every successful translation of the dislocation and is accomplished by removing all solute atoms at a distance in the x-direction equal to $W/2$ from the dislocation and replacing them with solutes at the same x-position but with randomly chosen y-coordinates. Simulation cell widths are chosen in such a way as to insure that this randomization has little effect on the system energy.

3. STATIC DISLOCATION RESULTS

To verify the present simulation procedure, we first examine the limiting case of solute segregation in the presence of a stationary edge dislocation. Analytical predictions are available for the segregation profile in this case. The solute distribution around a static dislocation and its images is expected to be asymmetric because the dislocation stress fields are anisotropic. Above the dislocation core, the pressure is compressive, while below the core it is tensile. We investigated several steady-state solute distributions for different initial concentrations. These simulations are performed on a 500 $\times$ 500 square lattice simulation cell. Figure 2 shows steady-state solute distribution around an edge dislocation for solute concentrations of 1% and 5%, with the quantity $Gb\Delta V(1+\nu)/[3H(1-\nu)kT] = 200$, where T is temperature and H is the height of the simulation cell (see Fig. 1).

Examination of Fig. 2 shows that there is net solute segregation to the dislocation in the form of a condensed atmosphere near the dislocation core and a more diffuse solute cloud farther away. The solutes tend to cluster under the dislocation core where the stress (pressure) is large and tensile because the solute misfit with respect to the matrix is positive, i.e. $\Delta V > 0$. Careful examination of the solutes in this condensed area around the core shows that every atomic site in this region is occupied by a solute atom (indeed, this is our definition of a condensed atmosphere). The density of solute atoms above the dislocation line is very small because the compression associated with the dislocation stress field raises the elastic energy of the systems there. Farther away from the dislocation, the solute distribution is more diffuse and forms a so-called Cottrell atmosphere [13].

To make these observations more quantitative, we construct a contour plot of the solute distribution and compare this directly with theoretical predictions (Fig. 3). The steady-state concentration profile around a dislocation is found using Boltzmann statistics as [15]

$$C = C_0 \exp\left(-\frac{P\Delta V}{kT}\right). \tag{4}$$

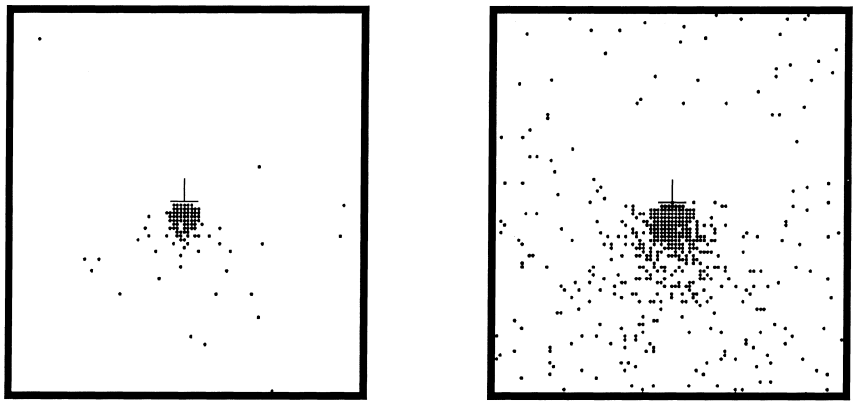

Fig. 2. Instantaneous image of the steady-state solute profile around a static edge dislocation at two different mean solute concentrations and for $Gb\Delta V(1+v)/[3H(1-v)kT] = 200$. Note the condensed solute cloud near the dislocation core.

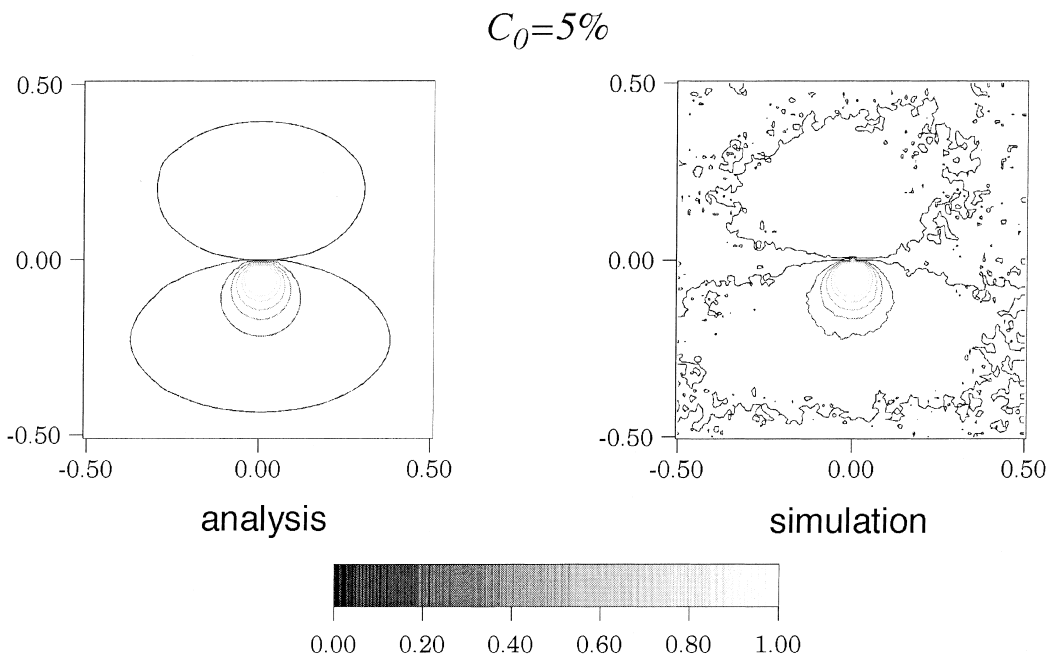

Fig. 3. Solute concentration contour plot obtained using the Fermi–Dirac analysis [left—equation (6)] and the simulation (right) for $C_0 = 5\%$ where $Gb\Delta V(1+\nu)/3H(1-\nu)kT] = 200$. The contour levels in both represent concentrations of C = 0.9, 0.8, 0.6, 0.4, 0.2, 0.03 and 0.01, from lightest to darkest. The noisy contours in the lower and upper halves of the simulation plot correspond to C = 0.03 and 0.01, respectively. The noisiness in these contours is associated with poor statistics at low concentrations.

Since the pressure diverges near the dislocation core, the concentration also diverges there. This is not possible in our simulations, since only one solute atom can occupy a single site at one time (i.e. the maximum value of c is unity). While this expression does not take this site exclusion into account, it may be included by switching from Boltzmann to Fermi–Dirac statistics [15]:

$$C = \frac{1}{1 + \left(\frac{1 - C_0}{C_0}\right) \exp\left(\frac{P\Delta V}{kT}\right)}. \qquad (5)$$

As is evident from Fig. 3, there is excellent agreement between the simulated (Fig. 2) and theoretical (Fermi–Dirac) solute distributions for the 5% solute case. In particular, both simulation and theory show the same condensed atmosphere below the dislocation line and a more diffuse cloud farther away from the dislocation line. The simulation contour plot in the low-concentration region is noisy because of the poor statistics associated with the small number of solute atoms. Additional simulations were performed for other lattice sizes, solute concentrations and temperatures and the same quality of agreement between simulation and theory was obtained.

4. DYNAMIC DISLOCATION RESULTS

In the previous section, we demonstrated that the simulated solute segregation to a stationary dislocation is in excellent agreement with theory. Before beginning the study of solute segregation to a moving dislocation, we validated the dislocation motion algorithm. To this end, we set the solute concentration to zero, applied various external stresses (σ_{xy}) and measured the steady-state dislocation velocity. This and all subsequent simulations were performed on a W = 2000 and H = 200 simulation cell. The dislocation velocity vs external stress is presented in Fig. 4 for the case of $Gb^2/kT = 200$ (i.e. low temperature). The dislocation velocity initially increases linearly with increasing external stress and then saturates at a fixed velocity at large stress.

The attempt rate for moving the dislocation is Γ and for each move the maximum displacement is one lattice spacing, i.e. b. Therefore, the maximum possible velocity in our simulation is $b\Gamma$. Since we attempt to move a dislocation by randomly choosing between the two possible directions along the glide plane, even in the limit of an infinite external stress, only half the attempted moves on average will result in motion of the dislocation along the direction selected by the stress. Putting all of these factors together, we expect a maximum or saturation velocity of $b\Gamma/2$. In the reduced units employed here, the saturation velocity is thus 1/2 (indicated by the broken line in Fig. 5). The simulation results are in excellent agreement with this prediction.

The second feature in Fig. 4 that can be predicted

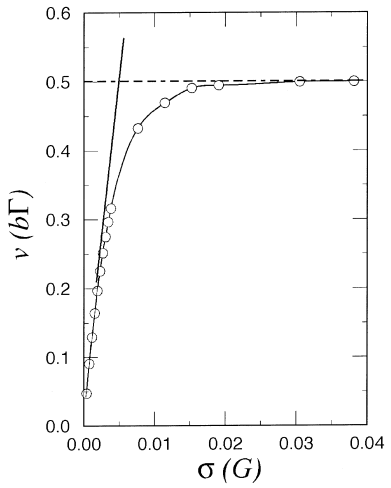

Fig. 4. Dislocation velocity vs external stress with no solute present. The straight, solid line is the predicted low-velocity mobility [equation 6(b)] and the dashed line represents the expected saturation velocity.

analytically is the slope of the velocity–stress curve in the low stress limit. The Einstein relation allows us to express the dislocation mobility in terms of the dislocation diffusivity, D (measured from the thermal root-mean-squared displacement of the dislocation with no impurities and no applied stress), as $M = D/(kT)$. The relation between the diffusivity and the dislocation attempt rate in one dimension (i.e. along the glide direction) is $D = \Gamma b^2/2$, where b is also the lattice parameter. Therefore, the dislocation mobility is $M = \Gamma b^2/(2kT)$ and the dislocation velocity is

$$v = MF = \left(\frac{1}{2}\frac{\Gamma b^2}{kT}\right)(\sigma b), \tag{6a}$$

and in the reduced units of Fig. 5 it is

$$\frac{v}{b\Gamma} = \left(\frac{1}{2}\frac{Gb^2}{kT}\right)\frac{\sigma}{G}. \tag{6b}$$

The term in parentheses is the theoretical slope of the curve and is shown in Fig. 4 as a solid line. Clearly, the velocity–stress data obtained from the simulations are in excellent agreement with this theoretical prediction.

We now examine the case of a moving dislocation interacting with diffusing solute atoms. In this part of the study, we focus on the evolution of the solute concentration profile as a function of stress and on the velocity–stress relation. In the simulation results reported below, we fix the following parameters: $Gb\Delta V(1+\nu)/[3H(1-\nu)kT] = 200$, solute concentration $C_0 = 7.5 \times 10^{-4}$, and the mobility ratio $M_r = 0.01$.

We first examine the solute distribution around the moving dislocation for a very small external stress $\sigma = 3.3 \times 10^{-4}G$ and $\Delta V = 0.5b^2$. Figure 5 shows the solute distribution after a long time ($t = 2.5 \times 10^7/\Gamma$). Clearly, the solute distribution appears random except near the dislocation line itself, where many solute atoms have accumulated beneath the dislocation line. The small square in this figure represents the region around the dislocation which is magnified in Fig. 6 at several different times during the same simulation run. At short times ($t = 2.5 \times 10^4/\Gamma$), the solutes are nearly randomly distributed (see the first image in Fig. 6). The dislocation has moved a short distance to lower its energy by translating to the position of the closest solute atom on its glide plane. At the next time shown ($t = 1.25 \times 10^7/\Gamma$), the dislocation has moved back by a few lattice spacings to take advantage of other solutes that have diffused towards the nearly stationary dislocation. In this case, the dislocation has already begun to form a condensed solute cloud at its core. In the final image in Fig. 6 ($t = 2.5 \times 10^7/\Gamma$), the dislocation has moved backwards a few more lattice spacings and the size of the condensed region at its core has grown. Clearly, at this very small external stress, the dislocation is easily pinned by the solute atoms and the longer it remains in its pinned location, the more solute atoms diffuse to it. As a result, the dislocation becomes more tightly pinned until the steady-state (near equilibrium) solute profile is achieved and the pinning saturates.

In the next simulation, we increased the external stress by two orders of magnitude to $\sigma = 2.0 \times 10^{-2}G$ and $\Delta V = 0.5b^2$. The resultant (instantaneous) solute configurations around the dislocation are shown in Fig. 7. At the earliest time in this figure ($t = 2.5 \times 10^4/\Gamma$), the dislocation has moved a large distance compared with that in the low-stress case (Fig. 6) and has accumulated very few solute atoms. At $t = 1.25 \times 10^7/\Gamma$, the dislocation has moved a distance nearly 1.5 times that of the simulation cell width (crossing the cell boundary once) and has accumulated a significant condensed

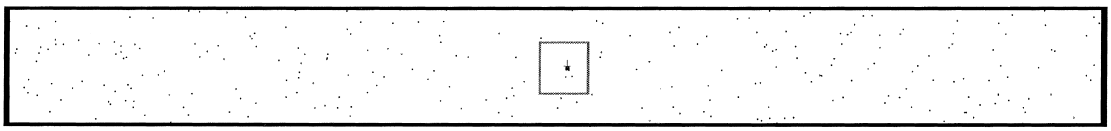

Fig. 5. The instantaneous solute distribution and dislocation position at $t = 2.5 \times 10^7/\Gamma$ during a simulation run with $\sigma = 3.3 \times 10^{-4}G$ and $\Delta V = 0.5b^2$. Note, far from the dislocation line, the solute field is sparse and nearly random.

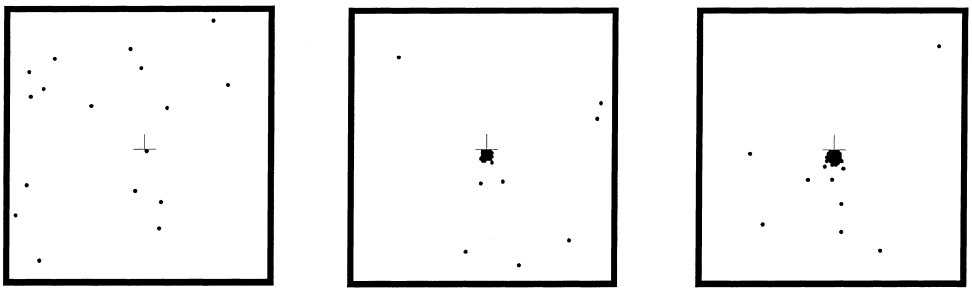

Fig. 6. Magnified view of the simulation cell around the dislocation at several times (t) during the simulation run shown in Fig. 5. The distance the dislocation has moved since the beginning of the simulation is Δx.

solute cloud. A comparison of the distance that the dislocation has traversed in its first 2.5×10^4 time steps with that in the subsequent 1.25×10^7 time steps suggests that the dislocation motion has greatly slowed because the dislocation has captured a substantial solute cloud. Upon doubling the simulation time (the last image in Fig. 7), the dislocation has only moved another $139b$ and has accumulated additional solute atoms. This suggests the existence of a feedback mechanism; solute accumulation slows dislocation motion and slower motion results in greater solute accumulation. This feedback mechanism operates until a self-consistent, steady-state solute distribution and velocity are obtained at a particular temperature, solute concentration and applied stress. In the steady state the dislocation moves by dragging its condensed solute cloud with it.

Finally, we show results for an external stress which is 65% larger than that represented in Fig. 7 (i.e. $\sigma = 3.2 \times 10^{-2}G$). Figure 8 shows that at this high stress, the dislocation moves at a relatively high velocity throughout the simulation run. At each time, the number of solutes around the dislocation core is very small and roughly time independent. In this case, the dislocation speed is sufficiently high that solute atoms are left behind, implying that the interaction between the dislocation and solute atoms is overwhelmed by high external stresses. It is interesting to note that although the applied stress would be large enough for the dislocation to reach its asymptotic value in the absence of solutes (see Fig. 4), its steady-state velocity here is less than 3% of that value. This retardation is somewhat surprising given the fact that no observable solute cloud forms.

The above discussion indicates that several distinct types of dislocation displacement–time behaviors are possible, depending on the magnitude of the applied stress. To quantify this relationship, we plot dislocation displacement vs time in Fig. 9 for the three values of the external stress already considered (Figs 5–8). At the lowest external stress level ($\sigma = 3.3 \times 10^{-4}G$), the dislocation initially translates quickly from its original position, moves back a short distance and then fluctuates about that position for the remaining $2.5 \times 10^7/\Gamma$. Although it is not possible to extract a meaningful velocity from

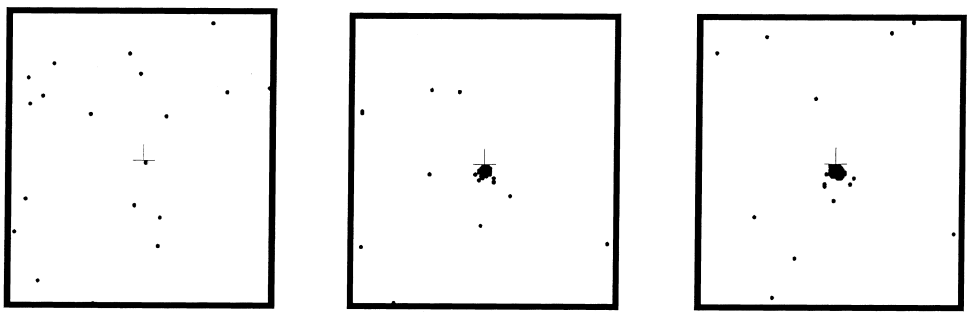

Fig. 7. Magnified view of the solute profile around the moving dislocation for the intermediate stress $\sigma = 2.0 \times 10^{-2}G$ and $\Delta V = 0.5b^2$.

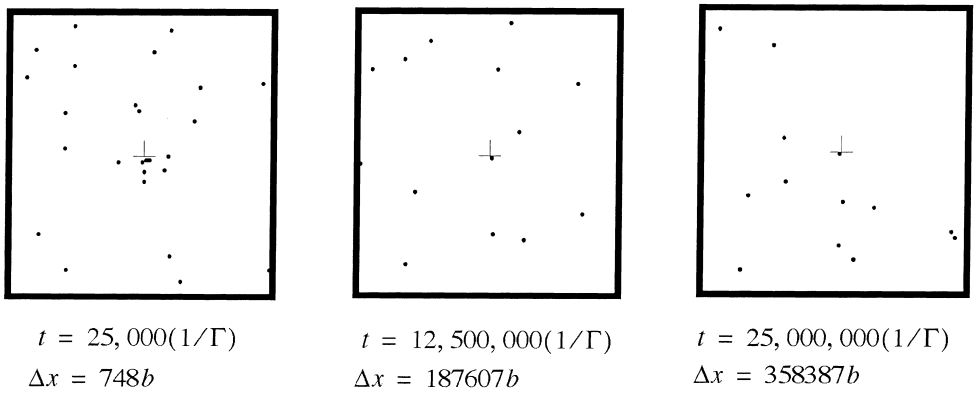

Fig. 8. Magnified view of the solute profile around the moving dislocation for the high stress $\sigma = 3.2 \times 10^{-2}G$ and $\Delta V = 0.5b^2$.

this non-monotonic curve, one can extract an approximate average velocity after the initial transient. At the intermediate stress level ($\sigma = 2.0 \times 10^{-2}G$), the dislocation moves with a relatively high velocity (in excess of 10^{-3} $b\Gamma$) at early times and then, at some critical time, abruptly slows to a relatively low velocity (10^{-5} $b\Gamma$)—a drop of approximately two orders of magnitude. Clearly the dislocation is captured here by solutes and subsequent motion only occurs by the dislocation dragging along its condensed solute cloud. At the highest stress ($\sigma = 3.2 \times 10^{-2}G$), the dislocation moves very quickly (in excess of 10^{-2} $b\Gamma$) during the course of the entire simulation, while crossing the boundary of the simulation cell nearly 200 times.

We now extract velocities from the plots in Fig. 9 (and from similar displacement–time plots for other stresses) and plot the resultant velocity–stress data in Fig. 10 for two values of the solute misfit parameter and, in addition, for the case with no solute. When the solute misfit is small, the presence of solutes makes little difference to the velocity–stress relationship, except for a small change in the effective dislocation mobility (i.e. the slope in Fig. 10 at small stress). This observation suggests that when the misfit is sufficiently small, the solute atoms exert a small, but finite drag on the dislocation. On the other hand, when the misfit is increased by a factor of five, the resultant velocity–stress relation is much different than in the solute-free system. In this latter case, the velocity is very small at low stress, but then increases rapidly at stress above approximately $0.03G$. It should be also noted that the velocity–stress relation is noisy over a small range of stress near $\sigma = 2 \times 10^{-2}G$.

The velocity–stress relation in the large misfit case ($\Delta V = 0.5b^2$) shown in Fig. 10 is replotted over a much larger range of stress in Fig. 11(a). This figure shows that, as in the solute-free and small misfit cases, the velocity asymptotes to the

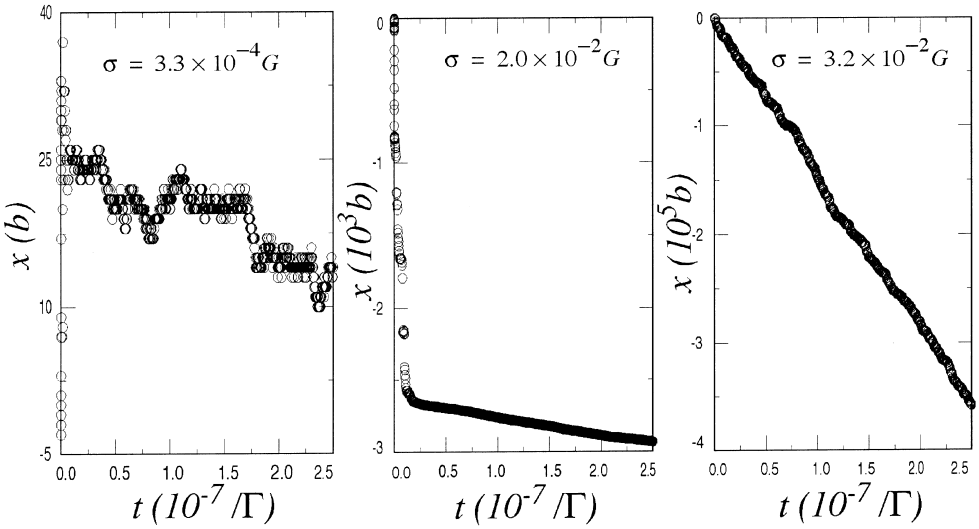

Fig. 9. Dislocation displacement vs time for the same stresses and misfit as in the three previous figures. Note the differences in the scales of the displacement axis.

same large stress limit ($v = 0.5b\Gamma$). By contrast, in this large misfit case, the velocity does not approach its asymptotic value until the stress is raised to nearly five times that of the solute-free case. Additionally, the maximum dislocation mobility (i.e. the slope in the v vs σ plot) is considerably smaller than the dislocation mobility when no solute is present. This result is in contradiction to earlier one-dimensional analytical work that suggests that once the dislocation pulls free of the solute, it asymptotically approaches the same mobility as in the solute-free case [5, 8, 9, 15]. One plausible explanation for this behavior is that the dislocation is randomly trapped and subsequently escapes from isolated solute atoms near its slip plane, giving rise to a stochastic pinning force.

Figure 11(a) also shows that the noise seen in the velocity–stress data near $\sigma = 2.5 \times 10^{-2}G$ appears to be associated with a bifurcation of the data into two distinct branches. This bifurcation occurs at a velocity that is within a factor of three of that predicted in earlier continuum solutions [13, 15, 16]. To clarify the velocity–stress behavior in this regime, we increase the magnification of the figure in the vicinity of $\sigma = 2 \times 10^{-2}G$ [see Fig. 11(b)]. At stresses less than $0.02G$, Fig. 11(b) shows that the dislocation velocity is very small, but finite. When the stress is raised above $0.022G$, individual simulation runs either show a similar small velocity or else a jump to a much higher value (several orders of magnitude larger). In fact, early in some simulations, the velocity will be on one velocity branch and then jump to the other at later times. The existence of two distinct branches over a finite range of stress suggest that the actual velocity has a stochastic nature. Further increases in stress lead to the disappearance of the low-velocity branch and a marked increase in the slope of the high-velocity branch of the velocity–stress curve [see Fig. 11(a)]. Thus, even when the dislocation pulls free of its solute cloud, it is still strongly influenced by the presence of solute atoms.

The origin of the jump in dislocation velocity is associated with the two types of dislocation motion that are operative—dislocation slip accompanied by solute drag and dislocation slip exceeding solute diffusion. The transition between these distinct regimes is likely the origin of the Portevin–LeChatelier effect, as is often argued [11, 12, 19, 20]. We note that while no quantitative theory of solute drag on moving dislocations that self-consistently describes the dislocation velocity and associated segregation profile is available, theoretical work on solutes interacting with migrating interfaces is closely related [2, 5, 6].

The critical or threshold stress σ_t that must be applied for the dislocation to escape from its solute cloud varies with solute concentration, C_0 (see Fig. 12). As more solute is added, the retarding force on the dislocation from the solute increases and a larger external stress must be applied for the dislocation to escape. Figure 12 demonstrates that the threshold stress is a nearly linear function of the solute concentration, where the threshold stress is pragmatically described as the highest stress for which the dislocation motion lies on the low-velocity branch [see Fig. 11(b)] in (at least three) simulations that run until a time of $t = 2.5 \times 10^7$ steps. Again, we note that the precise value of the critical or threshold stress determined here will be affected to some extent by the two-dimensional nature of the present simulations, which prevent dislocation line bow out between pinning obstacles.

When the external stress is low, the dislocation/solute interaction is strong, the solute content is large and/or the temperature is low, the dislocation can only move by dragging its solute cloud, as discussed above. The dislocation interacts most

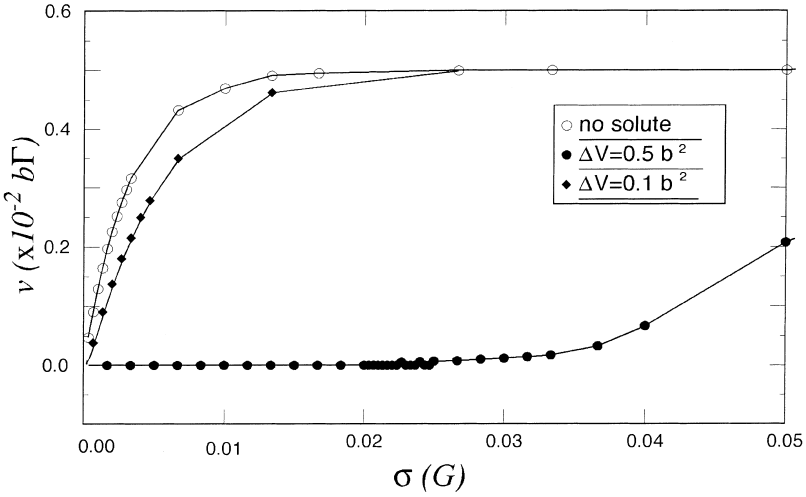

Fig. 10. Dislocation velocity vs external stress for the systems with no solute (open circle), large misfit solutes (solid circles) and small misfit solutes (solid diamonds).

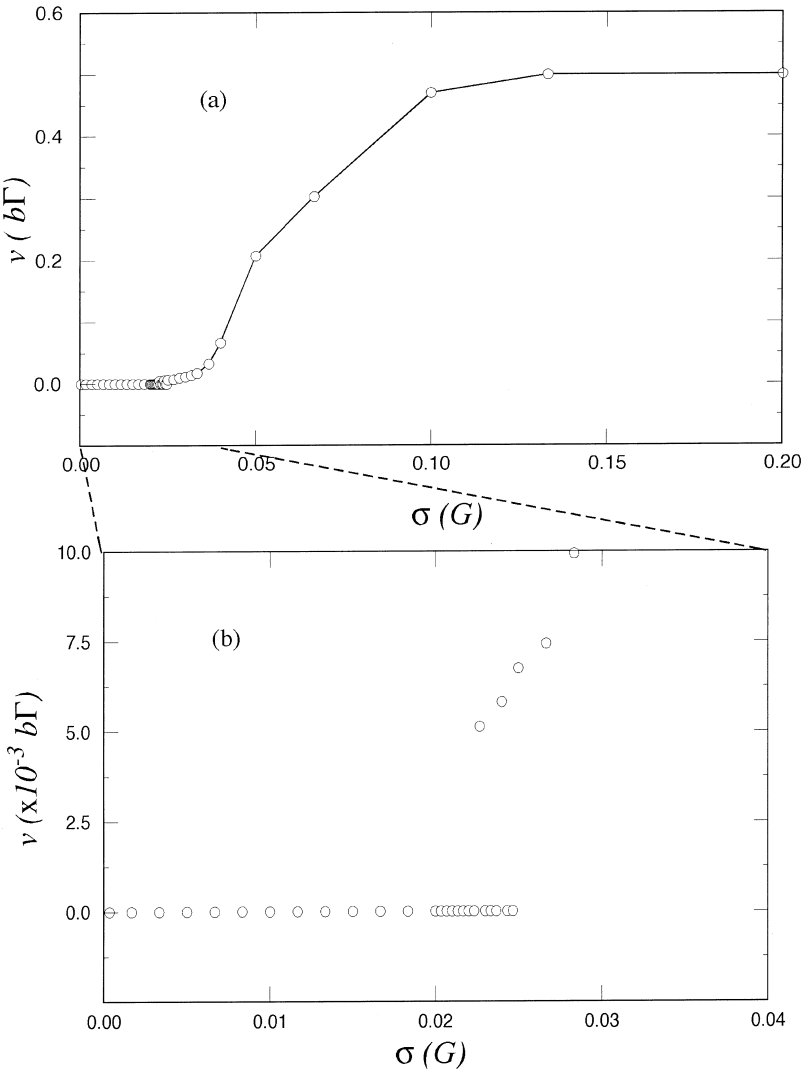

Fig. 11. Velocity vs external stress for the large misfit solute case of Fig. 10, (a) over a larger stress range than in Fig. 10 and (b) over a smaller stress range in the vicinity of the dislocation velocity bifurcation.

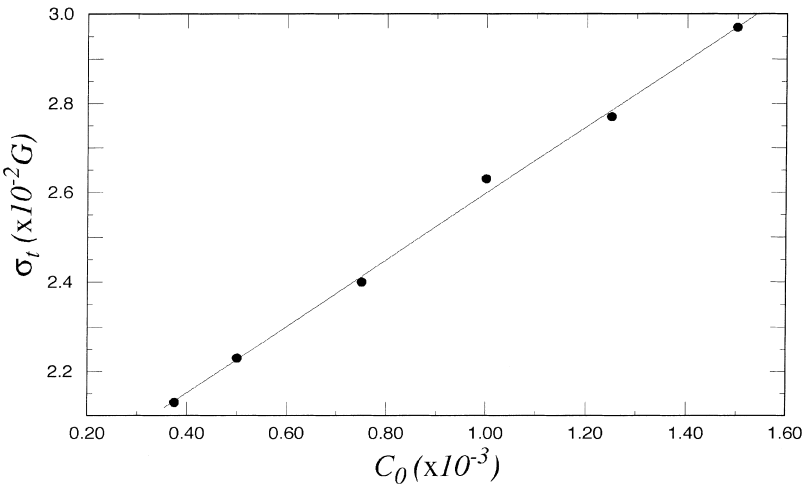

Fig. 12. Critical stress for unpinning the dislocation vs mean solute concentration.

strongly with the condensed solute cloud near its core. Although the present continuum model of the dislocation stress field is not accurate near the core (due to non-linear effects), this shortcoming is not important in the present context for two reasons. First, the stress field divergence near the core is cut off at one atomic spacing (i.e. a dislocation and a solute occupying the same site do not interact). Second, the size of the condensed solute cloud is controlled by the linear elastic stress field (provided the cloud radius is larger than an atomic spacing or two) and the overall dislocation–condensed solute cloud interaction is more sensitive to the size of the condensed cloud than the detailed behavior at the dislocation core.

Since the dislocation–solute interaction is dominated by the condensed solute atoms near the dislocation core, we now examine how the size of (i.e. the number of atoms in) the condensed region, n, varies with the average solute concentration C_0 at fixed externally applied stress (see Fig. 13). We define the size of the condensed solute cloud as the number of solute atoms that are contiguous with the dislocation (i.e. are connected to the dislocation line by a continuous path of solute atoms). Figure 13(a) shows that at low stress ($\sigma = 3.3 \times 10^{-4} G$), the size of the condensed cloud increases nearly linearly with average solute concentration. However, at higher stresses ($\sigma = 2.0 \times 10^{-2} G$), the solute cloud is very small at low concentrations, increases precipitously at a particular concentration and then rises approximately linearly with increased solute concentration [as it did at low stress—Fig. 13(a)]. This observation is related to the change from the low-velocity (small stress), solute-drag limited dislocation motion to the high-velocity, nearly solute-free motion at large stresses. In the present case, the abrupt change in

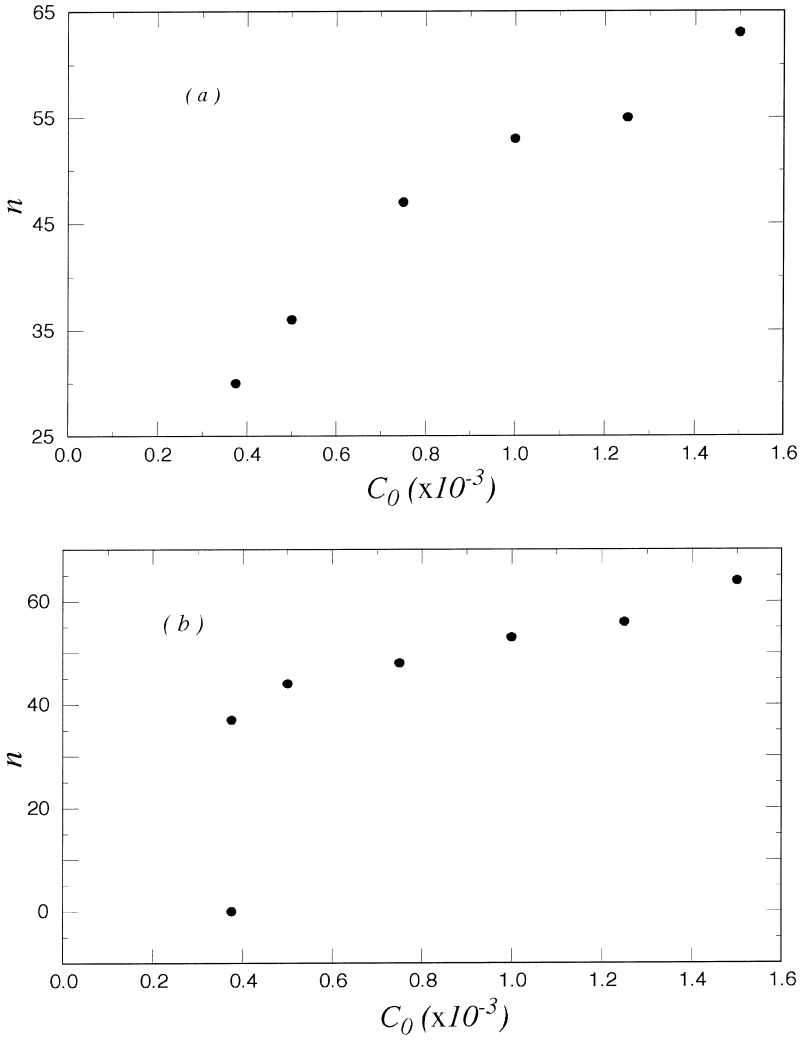

Fig. 13. The size of (number of atoms in) the condensed solute cloud, n, contiguous with the edge dislocation vs mean solute concentration C_0 at (a) $\sigma = 3.3 \times 10^{-3} G$ and (b) $\sigma = 2.0 \times 10^{-2} G$ for different initial concentrations.

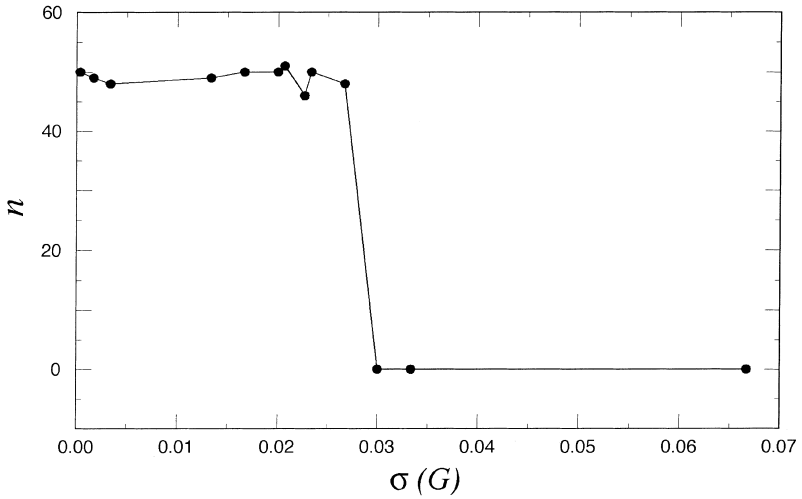

Fig. 14. The size of (number of atoms in) the condensed solute cloud, n, contiguous with the edge dislocation vs applied stress for $C_0 = 7.5 \times 10^{-4}$.

the size of the condensed cloud signifies the greater propensity of the dislocation to attract solute at high solute concentration rather than at low solute concentration. This rapid increase in n correlates with the relatively abrupt jump from the low-velocity (large condensed cloud) to the high-velocity (small solute cloud) branches. Figure 13(b) indicates that threshold concentration for an applied stress of $\sigma = 2.0 \times 10^{-2}G$ is approximately $C_0 = 0.38 \times 10^{-3}$.

Upon fixing the average solute concentration and varying the external stress, the size of the condensed solute cloud will also change. This is shown in Fig. 14, where the size of the condensed solute cloud drops abruptly at a particular value of the applied stress. This value of the applied stress correlates very well with the stress at which the velocity jumps to the high-velocity branch in Fig. 11 for the same solute concentration. However, it is not possible to distinguish whether the solute cloud size dropped because the velocity rose or vice versa. It is interesting to note that on the scale of Fig. 14, the size of the solute cloud is nearly independent of stress on either side of the threshold, suggesting that at both high and low stresses (i.e. away from the threshold stress) the retarding force associated with the condensed solute cloud is independent of the external stress.

5. CONCLUSIONS

We developed a discrete lattice, kinetic Monte Carlo model to simulate the motion of an edge dislocation in the presence of interacting, diffusing solute atoms that have a misfit with respect to the matrix. The simulation self-consistently determines the solute concentration profile in two spatial dimensions, as well as the dislocation velocity. In the cases of a dislocation moving in the absence of solute and solute segregation to a stationary dislocation, the Monte Carlo model was shown to accurately reproduce the classical results. The solute segregation profile around the moving dislocation is characterized at low (and zero) velocity (i.e. low stress) by a condensed solute cloud near (and on one side) of the dislocation core and a region depleted of solute on the opposite side. Further away from the dislocation, a much more diffuse solute (Cottrell) atmosphere is observed. Initially, the dislocation moves until it encounters a favorably located solute atom and becomes nearly pinned as additional solute atoms diffuse towards it—eventually resulting in a steady-state solute profile. Even with solute atoms segregated to the dislocation, the dislocation is able to move very slowly in response to the applied stress (i.e. it is limited by solute diffusion). At high velocity (high stress), no condensed solute cloud forms and the dislocation moves through the lattice with very little perturbation of the initially random solute distribution. In both the high- and low-velocity regimes, however, the dislocation mobility is perturbed by the presence of the solute. While this is expected at low velocity, the high-velocity results contradict the available simplified theories of dislocation motion in the presence of diffusing solute because of their neglect of stochastic dislocation core–solute interactions.

An intermediate velocity regime exists where dislocation motion can change abruptly with variations in stress and/or mean solute concentration. The velocity–stress diagram shows that two types of dislocation motion are possible in this regime at the same applied stress. The first is a low-velocity branch in which dislocation slip is limited by the diffusive motion of the condensed solute cloud. A high-velocity branch also exists where no solute condensation is observed. At stresses in this regime, we typically observe the dislocation being captured

by the solute atoms and, after a long time, pulling free and run at a velocity consistent with the high-velocity branch. This jump in velocity is shown to be coincident with an abrupt drop in the size of the condensed solute cloud. This suggests that dislocation motion in the presence of diffusing solute is hysteretic, as predicted by earlier one-dimensional theories. However, unlike the analytical predictions, here the dislocation velocity increases superlinearly with the applied stress, before saturating at high velocity. This unexpected finding is likely a result of the fact that even in the high-velocity regime, the dislocation stochastically encounters solute atoms which may be able to keep up with (and retard) the moving dislocation for a short time, before being lost again to the random solute field. This effect is strongest near the transition from one branch to the other and is expected to be negligible for very high-velocity dislocations.

The simulation approach developed herein is easily extendable to model the interaction between any moving line or planar defect and mobile point defects (impurities, vacancies, interstitials). It is also applicable to situations in which there are a large number of driven dislocations and hence may be used to model the Portevin–LeChatelier effect.

Acknowledgements—This work was supported by the US Department of Energy, Office of Basic Energy Sciences, Division of Materials Science. The work of R. LeSar was performed under the auspices of the US Department of Energy and that of J. Rickman with the support of NSF DMR-9975384.

REFERENCES

1. Mott, N. F. and Nabarro, F. R. N., *Proc. R. Soc.*, 1940, **52**, 86.
2. Dieter, G. E., in *Mechanical Metallurgy*. McGraw-Hill, New York, 1986, p. 203.
3. Nabarro, F. R., *Phil. Mag.*, 1977, **35**, 613.
4. Fogel, M. B., Trullinger, S. E., Bishop, A. R. and Krumhansl, J. A., *Phys. Rev. B*, 1979, **15**, 1578.
5. Cahn, J. W., *Acta. metall.*, 1962, **10**, 789.
6. Fukuyama, H. and Lee, P. A., *Phys. Rev. B*, 1978, **17**, 525.
7. Nakanishi, K., *J. Phys. Soc. Japan*, 1979, **46**, 1434.
8. Lücke, K. and Detert, K., *Acta metall.*, 1957, **5**, 628.
9. Srolovitz, D. J., Barnett, D. M., Eykholt, R. and Hirth, J. P., *Phys. Rev. B*, 1987, **35**, 6107.
10. Cottrell, A. H., in *Vacancies and Other Point Defects in Metals and Alloys*. Institute of Metals, London, 1958, p. 1.
11. Portevin, A. and LeChatelier, F., *C. R. Acad. Sci.*, 1923, **176**, 577.
12. Brindley, B. J. and Worthington, P. J., *Met. Mater.*, 1970, **4**, 101.
13. Cottrell, A. H. and Jaswon, M. A., *Proc. R. Soc. A*, 1949, **199**, 104.
14. Yoshinage, H. and Morozumi, S., *Phil. Mag.*, 1971, **23**, 1367.
15. Hirth, J. P. and Lothe, J., *Theory of Dislocations*. Wiley, New York, 1982.
16. Takeuchi, S. and Argon, A. S., *Phil. Mag.*, 1979, **40**, 65.
17. Fuentes-Samaniego, R., Gasca-Neri, R. and Hirth, J. P., *Phil. Mag.*, 1984, **49**, 31.
18. James, W. and Barnett, D. M., in *Solute-Defect Interaction—Theory and Experiment*. Pergamon, Oxford, 1986, pp. 136–142.
19. Cottrell, A. H., in *Relation of Properties to Microstructure*. American Society of Metals, Cleveland OH, 1954, p. 131.
20. Cottrell, A. H., *Phil. Mag.*, 1953, **44**, 829.